COMMUNICATIONS IN NUMERICAL METHODS IN ENGINEERING
Commun. Numer. Meth. Engng 2009; **25**:447–461
Published online 11 December 2008 in Wiley InterScience (www.interscience.wiley.com). DOI: 10.1002/cnm.1195

On quasi-steady laminar flow separation in the upper airways

A. Van Hirtum*, †, J. Cisonni and X. Pelorson

Gipsa-lab, Grenoble, France

SUMMARY

Accurate prediction of the position of flow separation along a constriction is important to model fluid–structure interaction phenomena in the upper airways such as phonation and obstructive sleep apnea. Flow assumptions underlying common flow descriptions along the upper airways are formulated. Flow separation positions obtained from theories with different degrees of complexity are qualitatively and quantitatively discussed. In particular, geometrical and flow features determining the influence of viscosity are varied. Increasing the constriction degree and the constriction length is shown to affect the position of flow separation. Boundary layer solutions and simulations with the two-dimensional Navier Stokes equations result in an accurate quantitative prediction of flow separation. Furthermore, Jeffery–Hamel flow solutions qualitatively predict the effect of both constriction height and length on the position of flow separation. The *ad hoc* assumption applied in quasi-one-dimensional flow descriptions does not accurately predict flow separation. Copyright © 2008 John Wiley & Sons, Ltd.

Received 15 May 2008; Revised 30 September 2008; Accepted 1 October 2008

KEY WORDS: two dimensional; laminar flow; phonation; obstructive sleep apnea; experimental validation

1. INTRODUCTION

Flow separation along the diverging part of a constriction is an important phenomenon when dealing with fluid–structure interactions. The upper airways anatomy extends from the glottis up to the lips and contains several constricted portions depending on the articulator positions. The interaction between soft tissues along constricted upper airway sites and respiratory airflow leads

*Correspondence to: A. Van Hirtum, Gipsa-lab, dpc, 961 rue de la houille blanche, BP46, Saint-Martin d'heres, 38402, France.
†E-mail: annemie.vanhirtum@gipsa-lab.inpg.fr

Contract/grant sponsor: French Ministry of Education and Research
Contract/grant sponsor: French Rhône-Alpes Regional Council
Contract/grant sponsor: Franco-British Partnership Programme Alliance
Contract/grant sponsor: Agence Nationale de la Recherche; contract/grant number: ANR-07-JCJC-0055

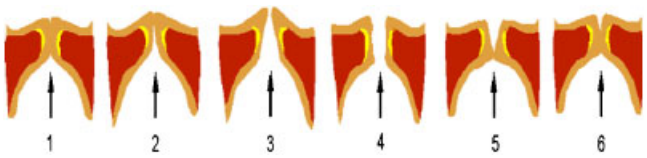

Figure 1. Characteristic variation of cross-sectional glottal profile during phonation, the arrow indicates the flow direction [1].

to some common daily and nightly life phenomena in normal as well as pathological upper airway conditions.

For healthy speakers, phonation or voiced sound production is due to a fluid–structure interaction between the vocal folds and expiratory airflow resulting in a rapid change of the glottal area as depicted in Figure 1 [1]. An example of a fluid–structure interaction occurring under pathological conditions is obstructive sleep apnea/hypopnea (OSA) [2]. OSA is characterized by intermittent cessation of breathing during sleep due to recurrent collapses of the pharyngeal airway. These collapses typically occur in pharyngeal airway portions with reduced cross-section e.g. between the tongue and hard palate [3].

Because, as will be demonstrated later, flow separation depends on the constriction geometry, the volume flow velocity is directly affected by its position. Furthermore, the pressure forces F_{wall}, exerted by the airflow on the surrounding pharyngeal walls, depend on the location of flow separation along the pharyngeal constrictions since

$$F_{\text{wall}} = \int_{\text{inlet}}^{\text{separation}} p(\bar{x})\,\mathrm{d}\bar{x} \tag{1}$$

Consequently, determination of flow separation is necessary in order to model upper airway phenomena as the varying glottal cycle during phonation or the collapse during OSA. Flow models with different degrees of complexity and accuracy are assessed in literature reflecting a trade-off between simplicity, accuracy, computational cost and physiological relevance. In general, limited computational cost and accuracy are important conditions for applications in clinical practice [4].

Simplified one and quasi-one-dimensional flow models are used in low-order physical vocal folds models to simulate phonation and estimate important phonation quantities, as e.g. auto-oscillation frequency and phonation onset threshold, at a minimum computational cost [5–7]. Two-dimensional flow models allow to increase the model accuracy while computational cost remains limited [8–12]. Important contributions to three-dimensional steady and unsteady modelling of flow through bifurcating lung branches and realistic oropharynx geometries with respect to quiet respiration are presented in a.o. [13–16].

In [15] it is concluded that locations of narrow flow passage should be the focus of any study aiming at understanding the human upper airway collapse. The need for experimental validation of flow simulations is stressed in [17]. Most simulation efforts deal with averaged geometries obtained during quiet breathing, consequently systematic variation of the constricted passage and flow conditions is of interest. Three-dimensional modelling of the impact of the geometry and flow circulation on the flow development with finite element modelling seems promising [18–21]. In particular, automatic mesh adaptation, as proposed in [18], is of interest considering modelling of the total fluid–structure interaction involving varying geometrical configurations in space and time. Nevertheless, the computational load of accurate three-dimensional modelling, requiring a

DOI: 10.1002/cnm

large amount of meshes, should not be underestimated and seems at current date out of reach for clinical applications.

The current study considers prediction of flow separation from steady two-dimensional laminar flow models with varying complexity. Important geometrical quantities such as constriction degree and length are varied. In addition, flow conditions are varied in a range significant to the upper airways during OSA and phonation. The assessed flow models are motivated and outlined. An experimental setup suitable for *in vitro* flow validation on mechanical replicas is presented and model predictions are discussed.

2. FLOW MODELLING IN THE UPPER AIRWAYS

2.1. In vivo geometry and flow conditions

Typical *in vivo* geometrical and flow conditions relevant for phonation and OSA are quantified in Table I. Based on the given orders of magnitude a dimensional analysis is performed. This yields a set of non-dimensional numbers that can be interpreted as a measure of the importance of various flow effects from which several flow assumptions can be formulated [23].

Following the characteristic aspect ratio ($h/W \ll 1$) the flow is assumed to be characterized by a bi-dimensional (2D) flow description in the (x, y)-plane with h being a typical minimum aperture and W a typical width. The resulting geometry is schematically presented in Figure 2. The geometry depicts the glottis during phonation, both walls are curved due to the presence of the vocal folds. In case the geometry represents the upper airways in supine position during OSA, the curvature is limited to the upper wall representing the tongue and the flat bottom wall represents the hard palate. Velocities involved during respiration and phonation are small compared with the speed of sound in air, so that the flow is assumed to be incompressible, i.e. squared Mach number $Ma^2 \ll 1$. Furthermore, the airflow is considered as primarily steady due to the low Strouhal number ($Sr \ll 1$). Finally, as a first approximation, the flow is assumed to be inviscid

Table I. Characteristic *in vivo* geometrical and flow conditions for phonation and OSA [9, 22].

Fluid properties of air		
ρ_0	Mean density	$1.2\,\mathrm{kg\,m^{-3}}$
μ_0	Dynamic viscosity coefficient	$1.5\times10^{-5}\,\mathrm{m^2\,s^{-1}}$
c_o	Speed of sound	$350\,\mathrm{ms^{-1}}$
OSA		
L_{os}	Tongue length	5 cm
W_{os}	Pharyngeal width	3 cm
h_{os}	Minimum aperture	2 mm
U_{os}	Flow velocity	$8\,\mathrm{ms^{-1}}$
f_{os}	Breathing frequency	0.25 Hz
phonation		
L_{gl}	Glottal length	6–9 mm
W_{gl}	Glottal width	14–18 mm
h_{gl}	Glottal height	0–3 mm
U_{gl}	Flow velocity	$10\text{–}40\,\mathrm{ms^{-1}}$
f_{gl}	Fundamental frequency of oscillation	100–200 Hz

DOI: 10.1002/cnm

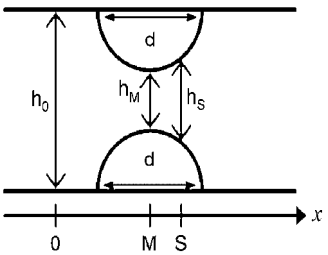

Figure 2. Schematic representation of the geometry with circular constriction of diameter d. The x-dimension indicates the flow direction. 0, M and s denote the positions of origin, minimum aperture and flow separation along the channel. The corresponding heights h_0, h_M and h_s (y-dimension) are indicated.

Table II. Non-dimensional numbers and flow assumptions: aspect ratio, Mach number Ma, Strouhal number Sr, Reynolds number Re_0.

	OSA	Phonation	Assumption
Aspect ratio	$h_{\mathrm{os}}/W_{\mathrm{os}} \ll 1$	$h_{\mathrm{gl}}/W_{\mathrm{gl}} \ll 1$	Two-dimensional
Ma^2	$10^{-4} \ll 1$	$10^{-2} \ll 1$	Incompressible
Sr	$10^{-3} \ll 1$	$10^{-2} \ll 1$	Steady
Re_0	$10^3 \ll 1$	$10^3 \ll 1$	Inviscid

considering characteristic Reynolds numbers ($Re_0 \gg 1$). Non-dimensional numbers and resulting assumptions are summarized in Table II for phonation and OSA.

2.2. *Viscosity and flow separation*

Although it can be neglected for the bulk flow considering Reynolds numbers Re_0, the occurrence of flow separation due to viscosity strongly influences the flow development. Therefore, flow separation cannot be neglected. In the studied flow models, the position of flow separation is determined either by an empirical *ad hoc* assumption or predicted based on vanishing wall shear stress, $\tau(x) = 0$, along the diverging portion of the wall where the flow is retarding, with

$$\tau(x) = \mu_0 \left(\frac{\partial u}{\partial y} \right)_{y=\mathrm{wall}} \tag{2}$$

and $u(x, y)$ the flow velocity within the boundary layer.

2.3. *Bernoulli with ad hoc viscosity correction*

Under the assumptions of one-dimensional, laminar, fully inviscid, steady and incompressible flow, one-dimensional Bernoulli's equation can be used to estimate the pressure and velocity distribution within a constriction. Bernoulli's equation is unable to account for flow separation and turbulent jet formation downstream of the minimum aperture h_M [24]. This phenomenon, resulting from very strong viscous pressure losses, must be taken into account in order to predict a pressure drop

DOI: 10.1002/cnm

along the constriction from one-dimensional Bernoulli theory. Therefore, an empirical criterion is required. The area associated with flow separation A_s is *ad hoc* set to $A_s = cA_M$, i.e. $h_s = ch_M$ with $c \geqslant 1$ the separation coefficient, for the 2D geometry with area $A(x) = Wh(x)$ as shown in Figure 2 [22]. The pressure distribution along the flow direction $p(x)$ is then derived from the upstream pressure p_0 and the geometry $h(x)$ as,

$$p(x) = p_0 + \frac{1}{2}\rho\frac{\Phi^2}{W^2}\left(\frac{1}{h_0^2} - \frac{1}{h(x)^2}\right) \tag{3}$$

$$\Phi = A_s\sqrt{\frac{2p_0}{\rho}} \tag{4}$$

where p_0 is the upstream pressure, ρ the fluid density, Φ the volume flow rate and h_0 the upstream channel height before the constriction. The volume flow rate is assumed to be constant along the constriction, i.e. $\Phi = U(x)A(x) = U(x)Wh(x) = \text{constant}$. Accounting for $h_0 \gg h_M$ and considering the pressure on the position of minimum aperture p_M results in:

$$p_M = p_0(1 - c^2) \tag{5}$$

Consequently, introducing an *ad hoc* constant c determines both the position of flow separation as well as the maximum pressure drop. Note that for the one-dimensional Bernoulli theory the position of maximum pressure drop coincides with the position of minimum aperture. Equation (5) can be used to estimate the constant c in order to match a measured pressure drop $p_0 - p_M$.

A quasi-one-dimensional flow description is obtained when further accounting for viscous effects in case of small Reynolds numbers. Small Reynolds numbers appear for small apertures h_M, e.g. toward closure in the glottal cycle or severe OSA. In order to account for viscosity, a Poiseuille term is added to Equation (3):

$$p(x) = p_0 + \frac{1}{2}\rho\frac{\Phi^2}{W^2}\left(\frac{1}{h_0^2} - \frac{1}{h(x)^2}\right) - 12\mu\frac{\Phi}{W}\int_0^x \frac{\mathrm{d}x}{h(x)^3} \tag{6}$$

The upstream pressure p_0 corresponds physiologically with the subglottal pressure in case of phonation or with the oral pressure in case of OSA. The quantities h_M and p_M correspond, respectively, to the aperture and the pressure at the minimum constriction point $x = M$. The straightforward physiological interpretation of the model quantities and limited computational cost are important arguments in favor of this simplified model approach. Moreover, the described flow model, with the *ad hoc* assumption in order to describe a movable flow separation position as a function of h_M, in combination with reduced mechanical models yields qualitative and quantitative predictions of important phonation characteristics, such as the minimum upstream pressure required to sustain auto-oscillations or the oscillation fundamental frequency [7]. The *ad hoc* constant c is commonly varied between 1.1 and 1.5 [22, 25].

2.4. *Jeffery–Hamel self-similar flow*

In this section flow between straight non-parallel walls with half-angle ω is considered assuming steady, laminar, two-dimensional, radial, incompressible and viscous flow in absence of external

DOI: 10.1002/cnm

forces. With these assumptions and radial velocity $u(r,\theta)$ the continuity equation and Navier Stokes equations in polar coordinates (r,θ) reduce to:

$$\frac{\partial u_r}{\partial r} = \frac{-u_r}{r} \tag{7}$$

$$\rho u_r \frac{\partial u_r}{\partial r} = -\frac{\partial p}{\partial r} + \mu \left\{ \frac{\partial}{\partial r}\left(\frac{\partial u_r}{\partial r} + \frac{u_r}{r} \right) + \frac{1}{r^2}\frac{\partial^2 u}{\partial \theta^2} \right\} \tag{8}$$

$$0 = -\frac{\partial p}{\partial \theta} + \frac{2\mu}{r}\frac{\partial u}{\partial \theta} \tag{9}$$

for which exact self-similar Jeffery–Hamel solutions can be obtained [23, 26–28]. Primarily because of the non-linearity of the differential equations multiple solutions are possible. In spite of the limiting assumptions, multiple solutions are of particular interest with respect to flow in the upper airways, since both symmetrical flow with separation and asymmetrical flow attachment to one of the walls are experimentally observed and extensively reported [29–34].

The equation of continuity can only be satisfied if the product ru_r is independent from θ. Therefore with $F(\eta)$ a normalized velocity profile function of $\eta = \theta/\omega$:

$$F(\eta) = \frac{u(r,\theta)}{u_{\max}(r)} \tag{10}$$

the momentum equations reduce to the non-linear ordinary differential equation for the normalized velocity profile $F(\eta)$:

$$F''' + 2\omega Re\, F F' + 4\omega^2 F' = 0 \tag{11}$$

with the boundary conditions:

$$F(-1) = 0, \quad F(0) = 1, \quad F(1) = 0 \tag{12}$$

The Reynolds number

$$Re = \frac{u_{\max} r \omega}{\nu} \tag{13}$$

is independent of r since $u_{\max} \propto 1/r$. The non-linear equation (11) can be solved either analytically, in terms of elliptical functions, or numerically, by a finite difference factorization scheme, for a given half-angle ω and Reynolds number Re. The skin-friction coefficient c_f is obtained from the solution $F(\eta)$ as

$$c_f = \frac{2|\tau_w|}{\rho u_{\max}^2} = \frac{2|F'(1)|}{Re} \tag{14}$$

So $F'(1)$ is a measure for the skin-friction coefficient. For diffusers and considering the slender-channel parameter $\omega Re > 0$ in the limit $Re \to \infty$ the skin-friction coefficient vanishes at $\omega Re = 10.3$. Therefore, although Jeffery–Hamel solutions are self-similar and cannot show flow separation, they are extremely suggestive in showing reversed flow near the walls for $\omega Re > 10.3$. Jeffery–Hamel solutions are used to approximately compute the flow in symmetric plane channels with weakly curving walls as well as to study flow stability [27, 35, 36].

DOI: 10.1002/cnm

2.5. Boundary layer solution

In the (quasi)-one-dimensional approach viscosity is either neglected (Equation (3)) or corrected for with an additional Poiseuille term, assuming fully developed Poiseuille flow (Equation (6)). However, at high Reynolds numbers Re_0, the region in which viscous forces are important is confined to a thin layer adjacent to the wall, referred to as laminar boundary layer. Outside the boundary layer, the inviscid irrotational main flow, with velocity $U(x)$, is described by Bernoulli's equation (3). The resulting boundary layer theory is described by the Von Karman momentum integral equation for steady flows [28]. An approximated method to solve this equation for laminar, incompressible, bi-dimensional (x, y) boundary layers is given by Thwaites method [37–39]. Two shape parameters are introduced

$$H(\lambda) = \frac{\delta_1}{\delta_2} \tag{15}$$

$$S(\lambda) = \tau \frac{\delta_2}{U} \tag{16}$$

which are only functions of the velocity profile determined by the acceleration parameter $\lambda \approx \mathrm{d}U/\mathrm{d}x\delta_2$ with wall shear stress $\tau(x)$, displacement thickness δ_1,

$$\delta_1(x) = \int_0^\infty \left(1 - \frac{u(y)}{U}\right) \mathrm{d}y \tag{17}$$

and momentum thickness δ_2,

$$\delta_2(x) = \int_0^\infty \frac{u(y)}{U} \left(1 - \frac{u(y)}{U}\right) \mathrm{d}y \tag{18}$$

The Von Karman equation is then approximated by:

$$\delta_2^2(x) U^6(x) - \delta_2^2(0) U^6(0) \propto \int_0^\infty U^5(x)\, \mathrm{d}x \tag{19}$$

Equation (19), in combination with the fitted formulas for $H(\lambda)$ and $S(\lambda)$ tabulated in [37], enables to compute the searched pressure distribution $p(x)$ up to the flow separation point x_s, where $\tau(x_s) = 0$, for a given input pressure and known geometry. Moreover, the point of flow separation x_s is numerically estimated, as separation is predicted to occur at $\lambda(x_s) = -0.0992$ [22]. Therefore, no *ad hoc* assumption needs to be made to account for flow separation, while the computational cost remains low.

2.6. Two-dimensional Navier Stokes

The two-dimensional continuity and Navier Stokes equations for steady, laminar and incompressible flow are

$$\frac{\partial u_x}{\partial x} + \frac{\partial u_y}{\partial y} = 0 \tag{20}$$

$$\rho_0 \left(u_x \frac{\partial u_x}{\partial x} + u_y \frac{\partial u_x}{\partial y}\right) = -\frac{\partial p}{\partial x} + \mu \left(\frac{\partial^2 u_x}{\partial x^2} + \frac{\partial^2 u_x}{\partial y^2}\right) \tag{21}$$

DOI: 10.1002/cnm

$$\rho_0\left(u_x\frac{\partial u_y}{\partial x}+u_y\frac{\partial u_y}{\partial y}\right)=-\frac{\partial p}{\partial y}+\mu\left(\frac{\partial^2 u_y}{\partial x^2}+\frac{\partial^2 u_y}{\partial y^2}\right) \tag{22}$$

where u_x and u_y denote the velocity component in the x and y dimension, respectively [28]. For reasons of symmetry, the upper half of the flow domain is discretized in finite elements and the commercial finite element software *ADINA CFD* is used as a solver [12, 40]. The upstream pressure p_0 is applied at the inlet. The no-slip boundary condition is set to the rigid wall, while the symmetry centerline is treated as a slip wall. The mesh density is increased in the constriction in order to accurately predict flow separation by considering vanishing wall shear stress.

3. EXPERIMENTAL SETUP

To enable *in vitro* experimental validation of the predicted pressure distribution, the setup schematically depicted in Figure 3 is used. Steady flow is provided by a valve controlled air supply (A) connected to a pressure tank of 0.75 m^3 (B) enabling to impose an airflow through a rigid constriction replica (D,E). An upstream pipe (C) of 95 cm connects the replica with the pressure tank. Pressure transducers (Endevco 8507C, Kulite XCS-093) are positioned in pressure taps upstream of the replica (F) and at the minimum constriction (G) in order to measure upstream pressure p_0 and pressure at the constriction p_M. The volume airflow rate Φ is measured (TSI4000) upstream of the replica (H). The constriction is formed by two rigid circular parts with radius 5 mm. Minimum apertures of 0.5 and 1.5 mm are experimentally assessed for p_0 ranging from 150 up to 1000 Pa.

4. FLOW SEPARATION PREDICTION

4.1. Bernoulli with ad hoc viscosity correction

The *ad hoc* assumption for flow separation and quasi-one-dimensional flow model outlined in Section 2.3 is commonly used as a flow description in physical phonation models [7, 22, 25, 41] for multiple reasons. Simplicity favors understanding and model analysis. Besides, the qualitative and quantitative predictive capacity of major phonation features is striking in spite of the simplicity. Furthermore, the relationship between model quantities and *in vivo* physiological meaningful quantities is unambiguous. Remark that all the models formulated in Section 2 require the upstream

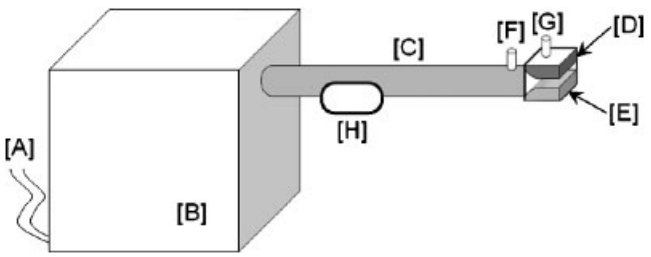

Figure 3. Schematic representation of the experimental setup: (A) air supply; (B) pressure tank; (C) upstream pipe; (D,E) rigid mechanical replica; (F,G) pressure taps; and (H) volume flow rate meter.

DOI: 10.1002/cnm

pressure p_0 as main input quantity. For phonation, p_0 corresponds *in vivo* to the subglottal pressure. Since *in vivo* non-invasive direct measurement of subglottal pressure is difficult to achieve, important *in vivo* applications as vocal fold pathologies might benefit from an alternative model formulation, in which the glottal pressure profile is derived from a downstream pressure instead of the upstream pressure. Such a formulation follows easily from Equation (5) relating p_0, p_M and the flow separation constant c analytically. Since the coefficient c determines both the separation position as well as the maximum pressure drop, it is interesting to assess the influence of a small variation in c on the estimated pressure $\widehat{p_m}$ and $\widehat{p_0}$ expressed by

$$\widehat{p_m} = p_0(1-c^2) \Rightarrow \left|\frac{\delta\widehat{p_m}}{p_0}\right| = |-2c\delta c| \tag{23}$$

$$\widehat{p_0} = \frac{p_m}{1-c^2} \Rightarrow \left|\frac{\delta\widehat{p_0}}{p_m}\right| = \left|\frac{2c\delta c}{(1-c^2)^2}\right| \tag{24}$$

with $\delta c = c - c_r$ denoting the discrepancy between the *ad hoc* assumed separation coefficient $c = \text{constant}$ and the coefficient corresponding to the actual separation position c_r. In phonation literature c is commonly choosen in the interval [1.1 1.5]. The outcome for $c = 1.2$ and $c_r \in [1\ 2]$ is illustrated in Figure 4. The lower limit $c_r = 1$ corresponds to separation at the constriction site whereas increased separation coefficients up to $c_r = 2$ can be expected whenever viscous effects dominate. It is seen that a small $\delta c = 0.1$ alters the estimated pressure to 24 and 125% of the input pressure. Consequently, the resulting pressure distribution and derived forces are severely influenced. Accounting for $\widehat{p_m}$ in $\widehat{p_0}$ as $\widehat{p_0} = \widehat{p_m}/1-c^2$ further increases the discrepancy. Therefore, although it is shown that the *ad hoc* separation assumption allows to characterize the flow behavior with a very low computational cost, more accurate flow models are required for which the position of flow separation does not impose the pressure drop. The same arguments hold in case of OSA where accuracy at a reasonable computational cost is required for surgical prediction purposes [9, 10].

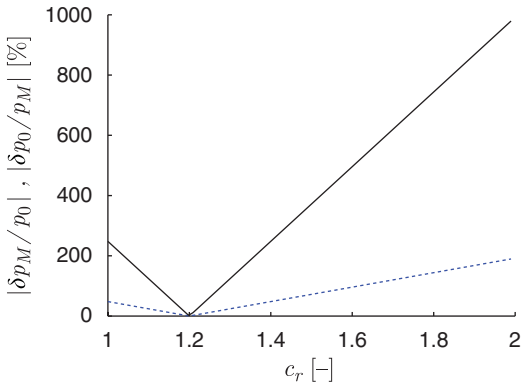

Figure 4. Error estimation related to flow separation c with upstream p_0 (dashed) or downstream (full) p_M pressure at minimum constriction as known input variable for *ad-hoc* assumption $c = 1.2$.

DOI: 10.1002/cnm

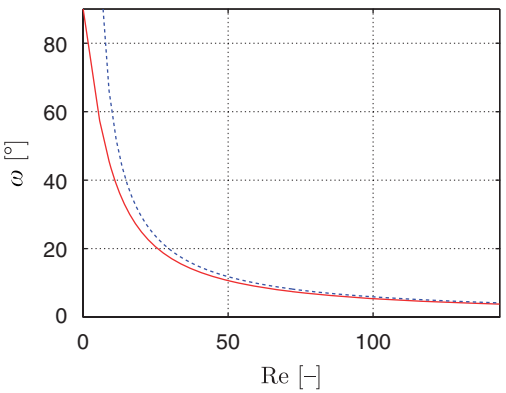

Figure 5. Analytical (full) and asymptotic (dashed) half angle ω corresponding to flow separation derived for a circular constriction with diameter $d=1\,\text{cm}$ and $h_M=1\,\text{mm}$.

4.2. *Jeffery–Hamel self-similar flow*

Jeffery–Hamel self-similar flow described in Section 2.4 is qualitatively assessed in terms of the main geometrical parameters d and h_M describing the circular constriction geometry depicted in Figure 2. In order to apply Jeffery–Hamel solutions, the circular geometry is locally approximated by its tangent from which a half angle ω is deduced. Analytically and asymptoticly obtained half angles $\omega(Re)$ corresponding to flow separation are illustrated in Figure 5. The asymptotic prediction $\omega Re=10.3$ is not valid for low Re. Consequently, except for low Re, both predictions coincide. Next, the parameter set (d, h_M) is varied within the range of interest for phonation and OSA, as reported in Table I. Resulting separation positions are expressed in terms of the parameter c, so that separation occurs at $h_s=ch_M$. Resulting $c(d, Re)$ and $c(h_M, Re)$ are illustrated in Figure 6(a). The diameter d is increased from 1 to 5 cm and the minimum aperture is set to $h_M=1\,\text{mm}$. In Figure 6(b) the minimum aperture h_M is increased from 0.2 up to 3 mm and the diameter is set to $d=1\,\text{cm}$. The separation coefficient c is seen to augment with increasing diameter d and decreasing minimum aperture height h_M due to the increasing influence of viscosity. Although qualitative tendencies are obtained, the velocity behavior expressed in Equation (10), i.e. $u\approx 1/x$, needs to be verified before assessing quantitative comparisons.

4.3. *Boundary layer solution and 2D Navier Stokes*

Flow separation is predicted from boundary layer solutions and 2D Navier Stokes simulations. The qualitative variations obtained from Jeffery–Hamel solutions for varying minimum constriction aperture h_M and diameter d are quantified. A circular geometry with diameter $d=1\,\text{cm}$, for which the upper half is illustrated in Figure 7, is assessed for $h_M=0.5$ and 1.5 mm. Predicted flow separation positions are illustrated in Figure 8. As a reference also flow separation coefficients estimated from measured upstream pressures p_0 and p_M, following Equation (5), are indicated. In addition the *ad hoc* assumption $c=1.2$ is shown. Measurements were made with the circular constriction mounted in the experimental setup described in Section 3 for $h_M=0.5$ and 1.5 mm. The upstream pressure p_0 was varied. Comparing the *ad hoc* assumption $c=1.2$ and $c=\sqrt{1-p_M/p_0}$ emphasizes the failure to predict both pressure drop p_M/p_0 and position of flow separation

DOI: 10.1002/cnm

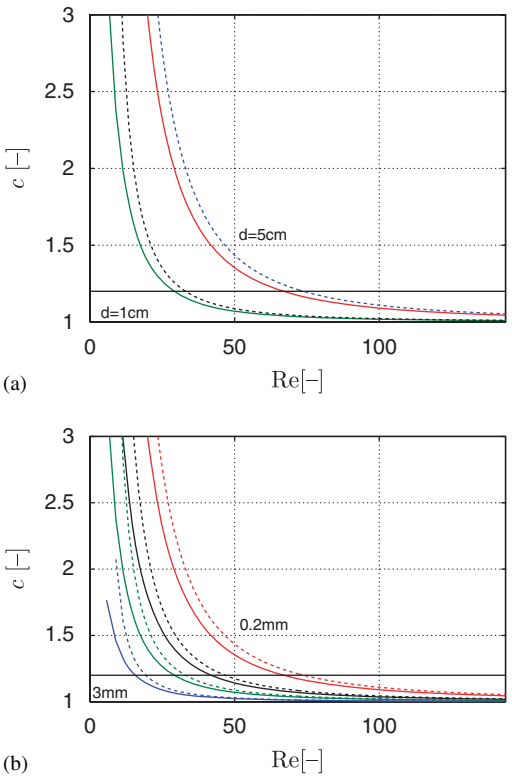

Figure 6. Analytical (full) and asymptotic (dashed) separation position expressed as $c = h/h_M$ on circular geometries for (a) diameter d set to 1 and 5 cm and minimum aperture $h_M = 1$ mm. *Ad hoc* $c = 1.2$ is indicated (straight line). (b) Corresponding separation position for $c = h/h_M$ on circular geometry with diameter $d = 1$ cm and increasing minimum aperture h_M 0.2, 0.5, 1.0 and 3 mm. *Ad hoc* is indicated $c = 1.2$ (straight line).

c using a single model parameter. For both apertures, $c = \sqrt{1 - p_M/p_0} \approx 1.05 < 1.2$, is yielded. Separation positions predicted from the boundary layer solutions systematically overestimate flow separation positions compared with values obtained with 2D Navier Stokes simulations. However, the difference remains within 3% regardless the upstream pressure and minimum aperture h_M. Consequently, both predictions match quantitatively. The predicted c values, associated with the position of flow separation, increase when the minimum aperture is decreased. This finding confirms the qualitative finding obtained with Jeffery–Hamel flow. The *ad hoc* coefficient $c = 1.2$ is seen to describe well the flow separation position for $h_M = 0.5$ mm and upstream pressures $p_0 > 400$ Pa. The value estimated from the measured pressure drop $c = \sqrt{1 - p_M/p_0}$ describes well flow separation positions for $h_M = 1.5$ mm.

The influence of the length of the constricted area on the position of flow separation is assessed with boundary layer solutions. The upstream pressure is as before varied from 150 up to 1000 Pa for $h_M = 0.5$ and 1.5 mm. The length of the constriction geometry remains 1 cm, but the constricted portion is extended by locally increasing the radius as shown in Figure 7. The influence on the flow separation position is illustrated in Figure 9. The predicted c values increase for both assessed

DOI: 10.1002/cnm

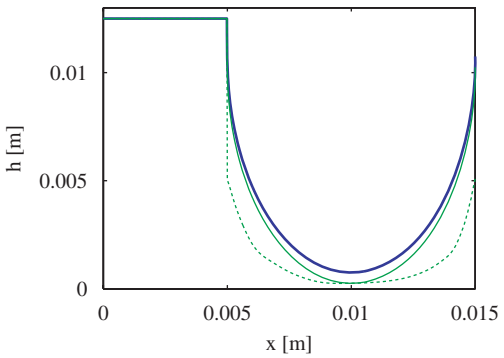

Figure 7. Upper half of the geometries: circular geometry $d=1\,\text{cm}$ with $h_M=0.5\,\text{mm}$ (full) and $h_M=1.5\,\text{mm}$ (thick full) and geometry with extended constriction length for which the minimum h_M remains at the same positions $h_M=0.5$ (dashed) and 1.5 mm (not shown).

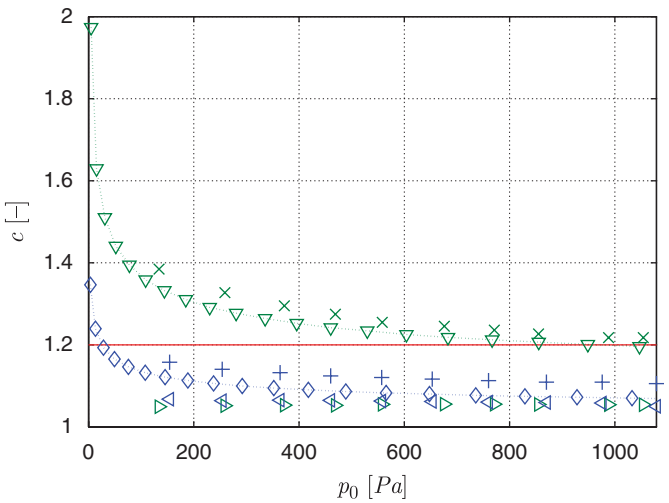

Figure 8. Flow separation position along a circular constriction with $d=1\,\text{cm}$ and $h_M=0.5$ and 1.5 mm predicted by boundary layer theory (0.5: $\times$ and 1.5: $+$) and 2D Navier Stokes (0.5: $\triangledown$ and 1.5: $\Diamond$). *Ad hoc* $c=1.2$ is indicated (straight line) as well as c matching measured ratios p_M/p_0 given by Equation (5) (0.5: $\triangleright$ and 1.5 $\triangleleft$).

minimum apertures h_M and in particular for the smallest, $h_M=0.5\,\text{mm}$, since viscous effects dominate. Quantitatively, c values increase with 4% for $h_M=1.5$ and with 7% for $h_M=0.5\,\text{mm}$. Increased c values confirm the qualitative finding outlined in Section 4.2.

5. CONCLUSION

Flow and geometrical conditions encountered in the human upper airways during phonation and obstructive sleep apnea lead to the assumptions of bi-dimensional, quasi-steady and laminar flow.

DOI: 10.1002/cnm

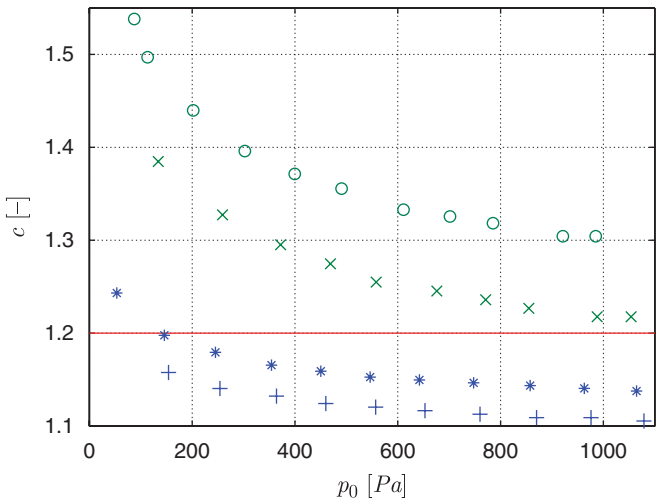

Figure 9. Flow separation position for $h_M = 0.5$ and 1.5 mm predicted by boundary layer theory for a circular geometry $d = 1$ cm (0.5: $\times$ and 1.5: $+$) and for an extended constricted region as shown in Figure 7 (0.5: $\circ$ and 1.5: $*$).

Flow models with different degree of complexity are assessed in order to model the position of flow separation along a constriction with varying minimum constriction aperture, constriction length and upstream pressure. Common quasi-one-dimensional flow models with an *ad hoc* separation criterion, frequently used in physical phonation modelling, are not suitable in case accurate predictions of both pressure drop and flow separation position are aimed due to the dependence of the pressure drop on the *ad hoc* assumption. Next, the dependence of the flow separation position on the minimum aperture and constriction length is qualitatively illustrated by considering Jeffery–Hamel flow. Jeffery–Hamel self-similar solutions, as exact solutions of the Navier Stokes equations, provide interesting features with respect to simulation validation and flow stability. Although, quantitative predictions are not assessed since further flow validation is needed. Moreover, due to the self-similarity, Jeffery–Hamel cannot be applied to all geometries. Nevertheless, the qualitative findings are confirmed by quantitative flow separation predictions obtained from boundary layer solutions and numerical simulations of the two-dimensional Navier Stokes equations. Both decreasing the minimum aperture and increasing the constriction length augment predicted c values, as a result of the increased importance of viscosity. Boundary layer solutions as well as simulations of two-dimensional Navier Stokes equations provide accurate prediction of the flow separation position. Clearly, boundary layer solutions limit computational cost in case *in-vivo* applications are aimed. The current systematic study of constriction length and height needs to be extended to more complex and realistic geometries. More complex flow models need to be considered, e.g. with respect to the occurrence of turbulence. Next, the ongoing flow–structure interaction should be modelled.

ACKNOWLEDGEMENTS

This work has been supported by a PhD grant from the French Ministry of Education and Research, by an Explora'Doc scholarship from the French Rhône-Alpes regional council, the Franco-British Partnership

DOI: 10.1002/cnm

Programme Alliance and Agence Nationale de la Recherche (ANR-07-JCJC-0055). The authors thank the anonymous reviewers for their helpful comments.

REFERENCES

1. Hirano M, Yoshida T, Kurita S. Anatomy and behavior of the vocal process. In *Laryngeal Function in Phonation and Respiration*, Baer T, Harris KS (eds). College Hill Press: Boston, MA, 1987; 1–13.
2. Young T, Palta M, Dempsey J, Skatrud J, Weber S, Badr S. The occurrence of sleep-disordered breathing among middle-aged adults. *New England Journal of Medicine* 1993; **17**(328):1230–1235.
3. Ayappa I, Rapoport DM. The upper airway in sleep: physiology of the pharynx. *Physiological Review* 2003; **7**:9–33.
4. Löhner R, Cebral J, Soto O, Yim P, Burgess JE. Applications of patient-specific CFD in medicine and life sciences. *International Journal for Numerical Methods in Fluids* 2003; **43**:637–650.
5. Ishizaka K, Flanagan JL. Synthesis of voiced sounds from a two-mass model of the vocal cords. *Bell System Technical Journal* 1972; **51**:1233–1267.
6. Ikeda T, Matsuzaki Y, Aomatsu T. A numerical analysis of phonation using a two-dimensional exible channel model of the vocal folds. *Journal of Biomechanical Engineering* 2001; **123**:571–579.
7. Ruty N, Pelorson X, Van Hirtum A, Lopez I, Hirschberg A. An in-vitro setup to test the relevance and the accuracy of low-order vocal folds models. *Journal of the Acoustics Society of America* 2007; **121**(1):479–490.
8. Wilquem F, Degrez G. Numerical modeling of steady inspiratory airflow through a three-generation model of the human central airways. *Journal of Biomechanical Engineering—Transactions of the ASME* 1997; **119**:59–65.
9. Van Hirtum A, Pelorson X, Lagrée PY. In vitro validation of some flow assumptions for the prediction of the pressure distribution during obstructive sleep apnoea. *Medical and Biological Engineering and Computation* 2005; **43**:162–171.
10. Chouly F, Van Hirtum A, Lagrée PY, Pelorson X, Payan Y. Numerical and experimental study of expiratory flow in the case of major upper airway obstructions with fluid–structure interaction. *Journal of Fluids and Structures* 2008; **24**:250–269.
11. de Vries M, Hamburg M, Schutte H, Verkerke G, Veldman A. Numerical simulation of self-sustained oscillation of a voice-producing element based on Navier–Stokes equations and the finite element method. *Journal of the Acoustics Society of America* 2003; **113**(4):2077–2083.
12. Cisonni J, Van Hirtum A, Luo XY, Pelorson X. Increasing the complexity of glottal flow models: in-vitro validation for steady flow conditions. *Proceedings of Acoustics08*, Paris, France, June 2008; 6.
13. Renotte C, Bouffioux V, Wilquem F. Numerical 3D analysis of oscillatory flow in the time-varying Laryngeal channel. *Journal of Biomechanics* 2000; **33**:1637–1644.
14. Zhao Y, Brunskill CT, Lieber BB. Inspiratory, expiratory steady flow analysis in a model symmetrically bifurcating airway. *Journal of Biomechanical Engineering—Transactions of the ASME* 1997; **119**:52–58.
15. Nithiarasu P, Hassan O, Morgan K, Weatherill NP, Fielder C, Whittet H, Ebden P, Lewis KR. Steady flow through a realistic human upper airway geometry. *International Journal for Numerical Methods in Fluids* 2008; **57**:631–651.
16. Xu C, Sin S, McDonough JM, Udupa JK, Guez A, Arens R, Wootton DM. Computational fluid dynamics modeling of the upper airway of children with obstructive sleep apnea syndrome in steady flow. *Journal of Biomechanics* 2006; **39**(11):2043–2054.
17. Heenan AF, Matida E, Pollard A, Finlay WH. Experimental measurements and computational modeling of the flow in an idealized human oropharynx. *Experiments in Fluids* 2003; **35**:70–84.
18. Chiandussi G, Bugeda G, Onate E. A simple method for automatic update of finite element meshes. *Communications in Numerical Methods in Engineering* 2000; **16**(1):1–19.
19. Arnold DN, Boffi D, Falk RS, Gastaldi L. Finite element approximation on quadrilateral meshes. *Communications in Numerical Methods in Engineering* 2001; **17**(11):805–812.
20. Zhang LT, Wagner GJ, Liu WK. Modelling simulation of fluid structure interaction by meshfree and FEM. *Communications in Numerical Methods in Engineering* 2003; **19**(8):615–621.
21. Carbonel CAAH, Galeao ACN. A stabilized finite element model for the hydrothermodynamical simulation of the Rio de Janeiro coastal ocean. *Communications in Numerical Methods in Engineering* 2007; **23**(6):521–534.
22. Pelorson X, Hirschberg A, Van Hasselt RR, Wijnands APJ, Auregan Y. Theoretical, experimental study of quasisteady-flow separation within the glottis during phonation. Application to a modified two-mass model. *Journal of the Acoustics Society of America* 1994; **96**(6):3416–3431.

DOI: 10.1002/cnm

23. Batchelor GK. *An Introduction to Fluid Dynamics*. Cambridge Mathematical Library: New York, 2000.
24. Stewartson K. D'Alembert's paradox. *SIAM Review* 1981; **23**:308–343.
25. Lucero JC. A theoretical study of the hystheresis phenomenon at vocal fold oscillation onset-offset. *Journal of the Acoustics Society of America* 1999; **105**(1):423–431.
26. Rosenhead L. The steady two-dimensional radial flow of viscous fluid between two inclined plane walls. *Proceedings of the Royal Society of London*, *Series A* 1940; **175**:436–467.
27. Fraenkel LE. Laminar flow in symmetrical channels with slightly curved walls. I. On the Jeffery–Hamel solutions for flow between plane walls. *Proceedings of the Royal Society of London*, *Series A* 1962; **267**:119–138.
28. Schlichting H, Gersten K. *Boundary Layer Theory*. Springer: Berlin, 1968.
29. Kucinschi BR, Scherer RC, DeWitt KJ, Ng TTM. Flow visualization and acoustic consequences of the air moving through a static model of the human larynx. *Transactions of the ASME* 2006; **128**:380–390.
30. Kucinschi BR, Scherer RC, DeWitt KJ, Ng TTM. An experimental analysis of the pressures and flows within a driven mechanical model of phonation. *Journal of the Acoustics Society of America* 2006; **119**:3011–3021.
31. Erath BD, Plesniak MW. The occurrence of the Coanda effect in pulsatile flow through static models of the human vocal folds. *Journal of the Acoustics Society of America* 2006; **120**:1000–1011.
32. Erath BD, Plesniak MW. An investigation of jet trajectory in flow through scaled vocal folds models with asymmetric glottal passages. *Experiments in Fluids* 2006; **41**:735–748.
33. Erath BD, Plesniak MW. An investigation of bimodal jet trajectory in flow through scaled models of the human vocal tract. *Experiments in Fluids* 2006; **40**:683–696.
34. Tao C, Zhang Y, Hottinger DG, Jiang JJ. Asymmetric airflow and vibration induced by the Coanda effect in a symmetric model of the vocal folds. *Journal of the Acoustics Society of America* 2007; **122**(6):2270–2278.
35. Banks WHH, Drazin PG, Zaturska MB. On perturbations of Jeffery–Hamel flow. *Journal of Fluid Mechanics* 1988; **186**:559–581.
36. Dennis SCR, Banks WHH, Drazin PG, Zaturska MB. Flow along a diverging channel. *Journal of Fluid Mechanics* 1997; **336**:183–202.
37. Blevins RD. *Applied Fluid Dynamics Handbook*. Krieger Publishing Company: Malabar, 1992.
38. Cebeci T, Cousteix J. *Modeling and Computation of Boundary-layer Flows*. Springer: Berlin, 2005.
39. Sobey IJ. *Introduction to Interactive Boundary Layer Theory*. Oxford University Press: New York, 2005.
40. Inc ADINA R&D. A.D.I.N.A. *Theory and Modeling Guide*: *Volume III*. ADINA CFD & FSI. Inc: Watertown, MA, U.S.A., 2006.
41. Lous NJC, Hofmans GCJ, Veldhuis RNJ, Hirschberg A. A symmetrical two-mass vocal-fold model coupled to vocal tract and trachea, with application to prosthesis design. *Acta Acustica* 1998; **84**:1135–1150.

DOI: 10.1002/cnm